

Transient stability versus damping of electromechanical oscillations in power systems with embedded multi-terminal VSC-HVDC systems

 ISSN 1751-8644
doi: 0000000000
www.ietdl.org

J. Renedo¹, L. Rouco², A. Garcia-Cerrada^{2,*}, L. Sigrist²

¹ ETSI ICAI, Universidad Pontificia Comillas, Madrid, Spain

² Instituto de Investigación Tecnológica (IIT), ETSI ICAI, Universidad Pontificia Comillas, Madrid, Spain

* E-mail: aurelio@iit.comillas.edu

Abstract: Multi-terminal high-voltage direct current technology based on voltage-source converter stations (VSC-MTDC) is expected to be one of the most important contributors to the future of electric power systems. In fact, among other features, it has already been shown how this technology can contribute to improve transient stability in power systems by the use of supplementary controllers. Along this line, this paper will investigate in detail how these supplementary controllers affect electromechanical oscillations, by means of small-signal stability analysis. The paper analyses two control strategies based on the modulation of active-power injections (P-WAF) and reactive-power injections (Q-WAF) in the VSC stations which were presented in previous work. Both control strategies use global signals of the frequencies of the VSC-MTDC system and they presented significant improvements on transient stability. The paper will provide guidelines for the design of these type of controllers to improve both, large- and small-disturbance angle stability. Small-signal stability analysis (in Matlab) has been compared with non-linear time domain simulation (in PSS/E) to confirm the results using CIGRE Nordic32A benchmark test system with a VSC-MTDC system. The paper analyses the impact of the controller gains and communication latency on electromechanical-oscillation damping. The main conclusion of the paper is that transient-stability-tailored supplementary controllers in VSC-MTDC systems can be tuned to damp inter-area oscillations too, maintaining their effectiveness.

Pre-print: J. Renedo, L. Rouco, A. Garcia-Cerrada, L. Sigrist, "Coordinated control in multi-terminal VSC-HVDC systems to improve transient stability: Impact on electromechanical-oscillation damping," arXiv:2208.00083, Online: <https://doi.org/10.48550/arXiv.2208.00083> (accessed 12-10-2022), pp. 1-17, 2022.

1 Introduction

Multi-terminal high voltage direct current systems based on voltage source converters (VSC-HVDC) is a key technology for bulk power transmission and for the integration of renewable resources into power systems [1–3]. This enabler technology has received attention worldwide [4] and several conceptual large VSC-HVDC grids have already been proposed in the literature. For example, in Europe, an HVDC-based *supergrid* has been proposed for bulk power transmission through different countries and integration of offshore wind energy [1, 2]. In North America, a *Macrogrid* consisting of several interregional HVDC interconnections has been proposed for massive integration of renewable energy sources [5, 6]. Similarly, an HVDC-based *hypergrid* has been proposed in Italy [7]. Meanwhile, actual examples of multi-terminal VSC-HVDC systems in operation in China are Zhoushan 5-terminal HVDC system [8], Nan'ao 3-terminal HVDC system [9–11] and Zhangbei 4-terminal system [12].

Although it is clear that the main application of VSC-HVDC systems is power transmission, they can also help to improve the operation of power systems by means of supplementary controllers [13, 14]. Previous publications have proposed supplementary controllers in multi-terminal VSC-HVDC systems (VSC-MTDC) to improve rotor-angle stability against small disturbances (electromechanical oscillations, i.e., power-oscillation damping, POD) and against large disturbances (transient stability).

The work in [15] proposed controllers in VSC-HVDC links to damp electromechanical oscillations (also known as power-oscillation-damping (POD) controllers), by modulating active-power

(P) through a VSC-HVDC link and reactive-power (Q) injections at both converter stations. The controllers were designed using on robust control techniques. The work in [16, 17] proposed POD controllers in VSC-MTDC systems, where the VSCs modulate their P injections using the information from a Wide Area Measurement System (WAMS). The work in [18] proposed POD controllers in DC-voltage-droop-controlled VSC-MTDC systems. In this control strategy, one converter of the VSC-MTDC changes its DC-voltage set point proportionally to the locally measured frequency deviation, using the concept of DC-voltage loop shaping. The work in [19] proposed POD controllers in VSC-MTDC systems to modulate P and reactive-power (Q) injections of the VSCs and using global measurements of the frequencies at the connection points of the VSC stations of the MTDC system. Reference [20] proposed POD controllers in a VSC-HVDC link embedded in an AC grid based on Linear Matrix Inequality (LMI) optimisation and modulating P/Q injections at the converter stations. POD controllers in VSC-MTDC systems of the references discussed above presented promising results.

The improvement of transient stability of a power system using a VSC-MTDC system has already been addressed in the literature. The work in [21] proposed a control strategy in VSC-MTDC systems for transient-stability improvement, where VSC stations control their P injections based on a bang-bang controller and using the speed deviations of the generators with respect to the speed of the centre of inertia (COI) as input signals. Reference [22] proposed controlling P injections of the VSC stations of a MTDC system based on a sliding-mode strategy and also using global measurements. The work in [23] proposed a control strategy where VSC stations controlled their P injections, using global measurements of the frequencies of the

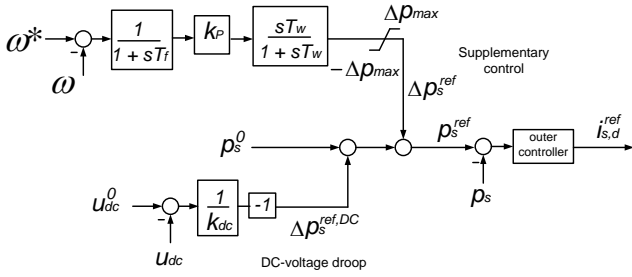


Fig. 2: Strategy P-WAF. Frequency in pu.

as in (1). The controller is activated only if the AC voltage at the connection point is above a certain threshold V_{TH} ($\gamma = 1$ if $u_s \geq V_{TH}$), to guarantee the control actions only after the fault is cleared (preventing the controller acting during a short circuit). This precaution improves the performance of the controller.

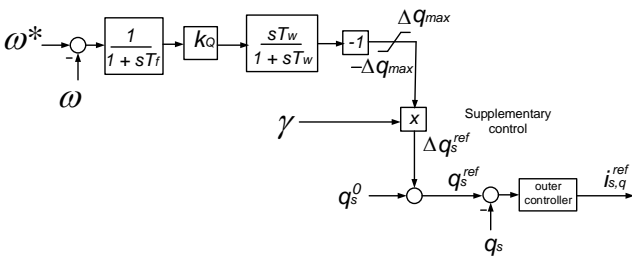


Fig. 3: Strategy Q-WAF. Frequency in pu.

The work in [25] used the following design:

$$\frac{k_{Q,k}}{k_{Q,T}} = \alpha_k, \quad k_{Q,T} = \sum_{j=1}^n k_{Q,j}. \quad (3)$$

4 Results

The case study considered consists of the CIGRE Nordic32A benchmark test system [39] with a 3-terminal VSC-HVDC system, as shown in Fig. 4. Each VSC has a nominal apparent power of 1000 MVA. A critical scenario with poorly damped inter-area oscillations is considered. The modifications made to stress the system and the data of the VSC-MTDC system are provided in the Appendix.

Each VSC of the MTDC system is controlled with DC-voltage droop control and constant reactive power injection. Table 1 depicts the initial steady-state operating point of the VSC-MTDC system, calculated with an AC/DC power flow [34, 35].

Table 1 Initial operating point of the VSC-MTDC system.

Converter	$P_{s,i}^0$ (MW)	$Q_{s,i}^0$ (MVar)	$u_{s,i}^0$ (pu)	$u_{dc,i}^0$ (pu)
VSC1	-350.00	0.00	1.0100	1.0006
VSC2	500.00	150.00	0.9982	0.9978
VSC3	-190.08	0.00	1.0149	1.0000

The dynamic model of the system in Fig. 4 has been linearised around the steady-state operation point and the linearised model has been implemented in Matlab-based Small Signal Stability Tool

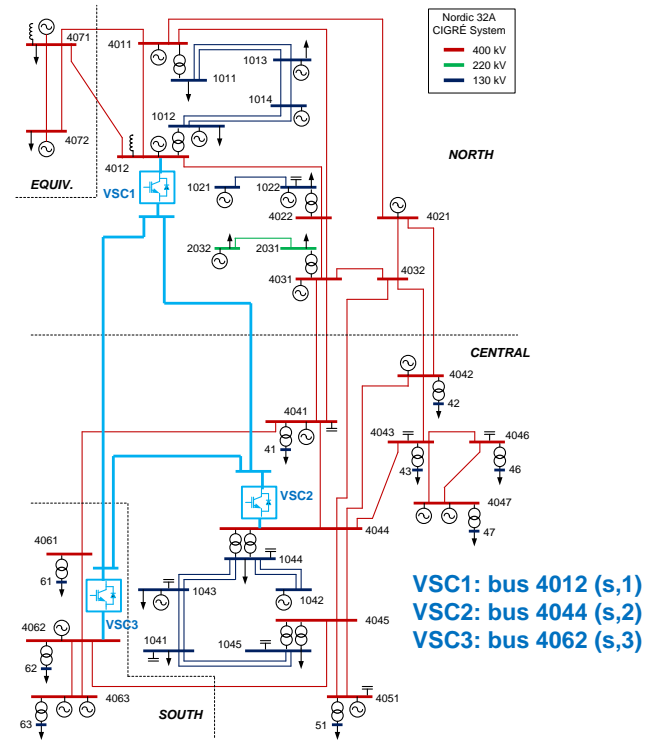


Fig. 4: Nordic32A system with a VSC-MTDC system.

(SSST) [40], as described in [28]. The linearised system reads:

$$\Delta \dot{\mathbf{x}} = \mathbf{A} \Delta \mathbf{x}. \quad (4)$$

where $\mathbf{A} \in \mathbb{R}^{n_x \times n_x}$ is the state matrix, $\Delta \mathbf{x} \in \mathbb{R}^{n_x \times 1}$ is the vector of increments of the state variables and n_x is the number of state variables of the system.

Electromechanical oscillations have been identified using eigenvalue techniques and participation-factors [41–43]. The system has two inter-area modes with low damping ratios, as depicted in Table 2.

Table 2 Inter-area modes.

Mode	Eigenvalue (rad/s)	ζ (%)	Freq. (Hz)	Dominant machines	Oscillation
A	$-0.1044 \pm j3.2333$	3.23	0.51	G4072, G4063	North against South & Centre
B	$-0.3186 \pm j5.2160$	6.10	0.83	G4063, G4072, G1042	North and South against Centre

The information about the electromechanical oscillations between different synchronous machines in the system can be extracted from the right eigenvectors of the linearised system (4), which are known as mode shapes [44]. The right eigenvector $\mathbf{v}_k \in \mathbb{C}^{n_x \times 1}$ associated to eigenvalue λ_k satisfies:

$$\lambda_k \mathbf{v}_k = \mathbf{A} \mathbf{v}_k. \quad (5)$$

The information of the oscillation of mode λ_k of a certain state variable of (4), x_i , can be analysed with the position of the right eigenvalue associated to the state variable $v_{ik} \in \mathbb{C}$. In particular, the phases of the mode shapes v_{ik} provide information about which state variables oscillate together with or against to other state variables, when a certain mode is excited.

Figs. 5 and 6 show the shapes of inter-area modes A and B (right eigenvectors associated to the speeds of the synchronous machines), respectively. In inter-area mode A, synchronous machines in the

North oscillate against synchronous machines in the South and in the Centre: mode shapes of the speeds of the generators in the North have opposite phases to mode shapes of the speeds of the generators in the South. In inter-area mode B, synchronous machines in the North and South oscillate against machines in the Centre: mode shapes of the speeds of the generators in the North and South are in phase, while they have opposite phases to mode shapes of the speeds of the generators in the South.

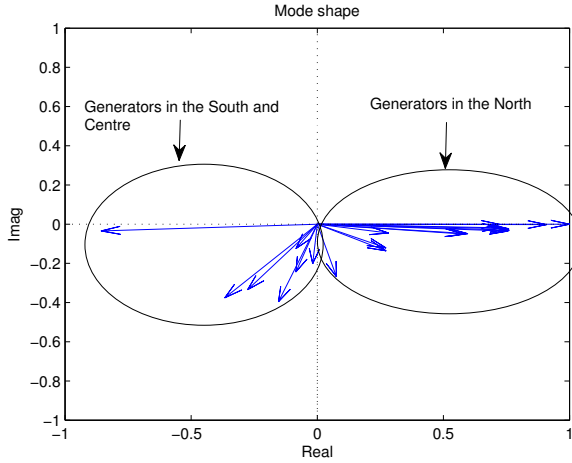


Fig. 5: Shapes of inter-area mode A.

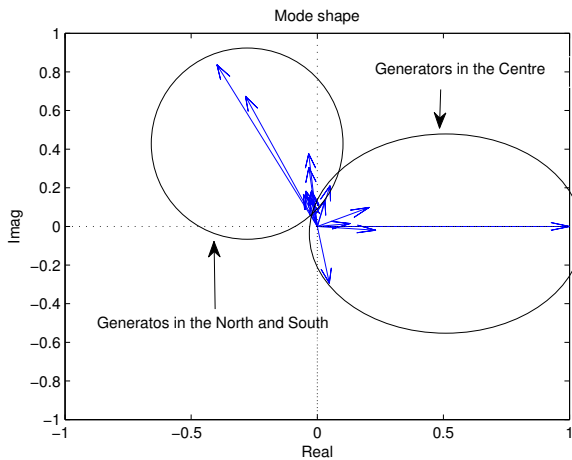


Fig. 6: Shapes of inter-area mode B.

4.1 Small-signal stability analysis

The impact of the controller gains of strategies P-WAF (P injections) and Q-WAF (Q injections) on inter-area modes is analysed. Gains at all VSC stations were changed (satisfying (2) and (3)) and eigenvalues and their damping ratio were obtained. Since gains in the range $k_{P,i}, k_{Q,i} = [100, 300]$ pu (pu's are referred to the converter rating) proved to be effective to improve transient stability [23, 25]. Now gains $k_{P,i}, k_{Q,i} = [0, 500]$ pu will be explored. The rest of parameters of the control strategies are provided in the Appendix.

Fig. 7 shows the evolution of the inter-area modes of the system and their damping ratios as the gains of control strategy P-WAF (P injections) increase. Initially, inter-area mode A moves towards the left-hand side of the complex plane as $k_{P,i}$ increases. However, for

high values of the controller gains this trend changes. The damping ratio of inter-area mode A increases as $k_{P,i}$ increases, it reaches its maximum value with $k_{P,i}$ around 200 pu. Inter-area mode B follows a similar pattern. The damping ratio of inter-area mode B increases as $k_{P,i}$ increases and it approximately saturates with $k_{P,i}$ around 300 pu. The damping ratios of inter-area modes A and B are much higher than the ones obtained in the base case, for all values of the controller gain $k_{P,i}$. In addition, notice that controller gains $k_{P,i}$ have small impact on the damping ratio of other modes.

Fig. 8 shows the evolution of the inter-area modes of the system and their damping ratios as the gains of control strategy Q-WAF (Q injections) increase. Inter-area mode A moves towards the left-hand side of the complex plane as $k_{Q,i}$ increases and its damping ratio increases, significantly. Inter-area mode B also moves towards the left-hand side of the complex plane as $k_{Q,i}$ increases and its damping ratio also increases. However, the damping ratio of mode B is lower than the one of mode A and saturates. Therefore, controller gains $k_{Q,i}$ have small impact on the damping ratio of other modes.

Results prove that with reasonable values of the controller gains for transient-stability improvement in strategies P-WAF and Q-WAF (e.g. $k_{P,i} = k_{Q,i} = 200$ pu), inter-area modes are also damped successfully without affecting other modes significantly. Furthermore, small-signal stability techniques can be used to design the controller gains in order to obtain the required damping ratios of the electromechanical modes.

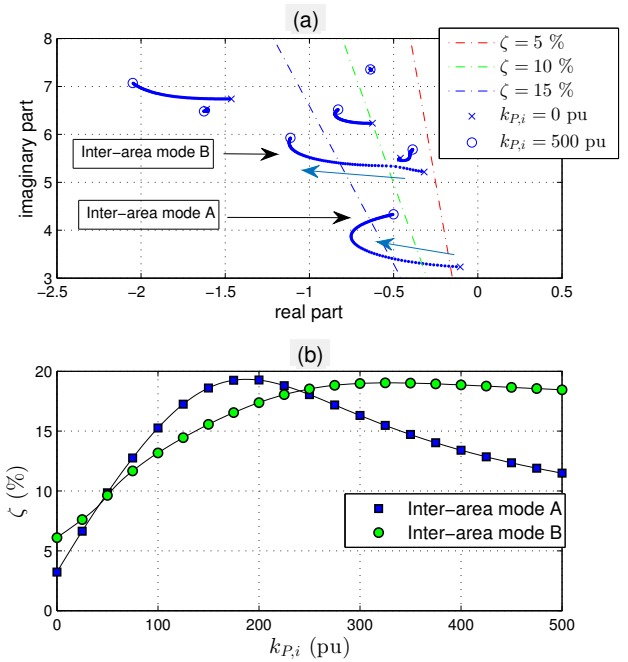


Fig. 7: Strategy P-WAF. Impact of gains $k_{P,i}$ on (a) evolution of electromechanical modes and (b) damping ratio.

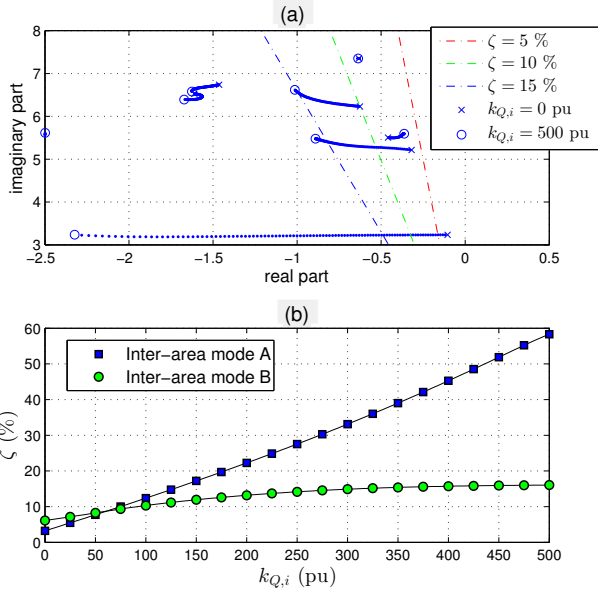


Fig. 8: Strategy Q-WAF. Impact of gains $k_{Q,i}$ on (a) evolution of electromechanical modes and (b) damping ratio

4.2 Non-linear time-domain simulation

The performance of the control strategies has been tested by means of non-linear time domain simulation in PSS/E tool (electromechanical simulation), using the model proposed in [34]. Four cases are compared:

- Base case: no supplementary control strategy.
- P-WAF: Strategy P-WAF (P injections) (Fig. 2), with $k_{P,i} = 200$ pu.
- Q-WAF: Strategy Q-WAF (Q injections) (Fig. 3), with $k_{Q,i} = 200$ pu.
- PQ-WAF: Simultaneous modulation of P and Q injections with strategies P-WAF and Q-WAF, with $k_{P,i} = k_{Q,i} = 200$ pu.

The rest of parameters of the control strategies are provided in the Appendix.

Line 4012-4022 (see Fig. 4) is tripped at $t = 1$ s. Fig. 9 shows the difference between the bus-voltage angles of generators 4072 (North) and 4063 (South). The three control strategies (P-WAF, Q-WAF and PQ-WAF) succeed in damping the inter-area oscillations present in the base case.

Figs. 10 and 11 show the active- and reactive-power injections of the VSC stations, respectively. In strategy P-WAF, only P injections are modulated. After the event, the P injection of VSC 1 decreases (P absorption of VSC 1 increases) because its frequency is above the WAF, while the P injections of VSCs 2 and 3 increase because their frequencies are below the WAF (see Fig. 12, as an example). Analogously, in strategy Q-WAF, only Q injections are modulated. The behaviour of Q injections in Q-WAF is similar to the behaviour of P injections in P-WAF, but with opposite direction, due to the negative sign of Fig. 3. In strategy PQ-WAF, both, P and Q injections are modulated. Both, modulation of P and/or Q injections of the VSC stations contribute positively to damp inter-area oscillations.

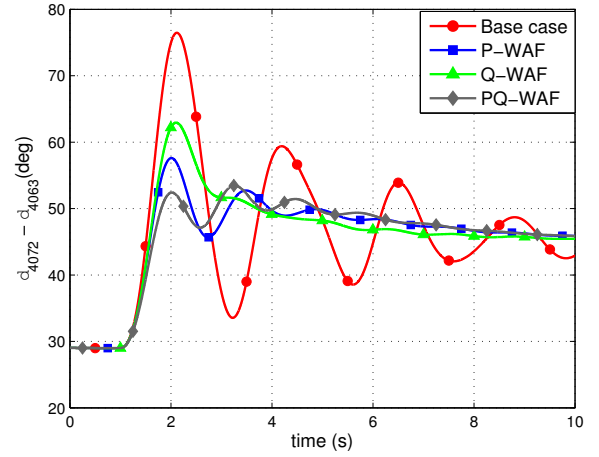


Fig. 9: Difference of generator angles.

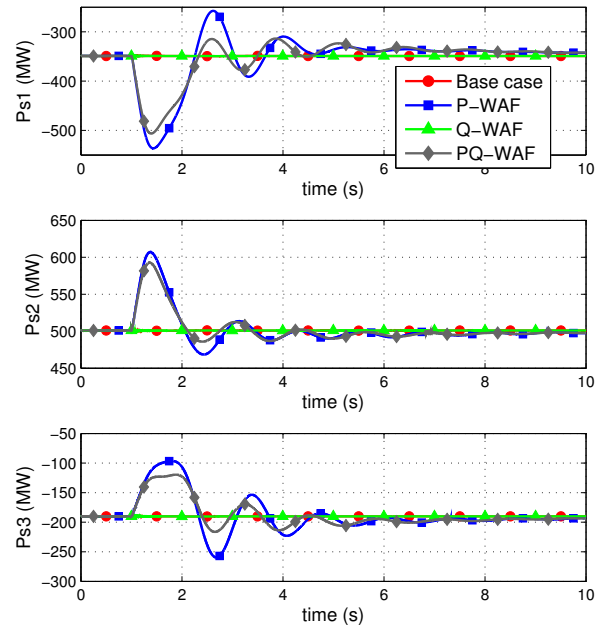


Fig. 10: Active-power injection of each VSC ($P_{s,i}$).

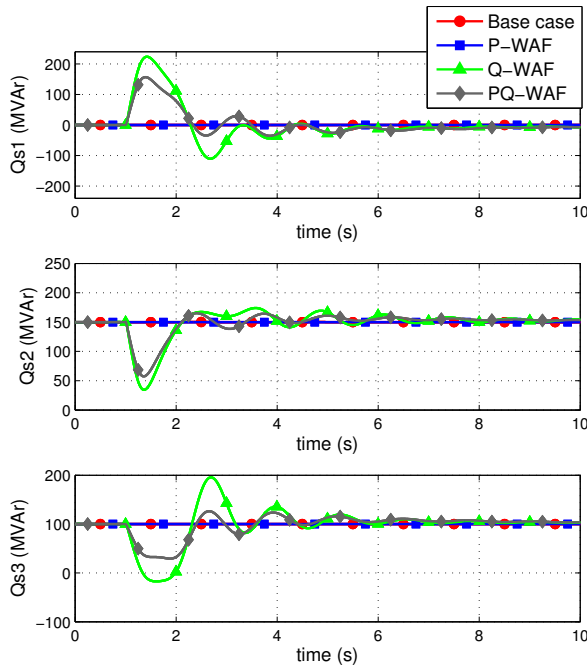


Fig. 11: Reactive-power injection of each VSC ($Q_{s,i}$).

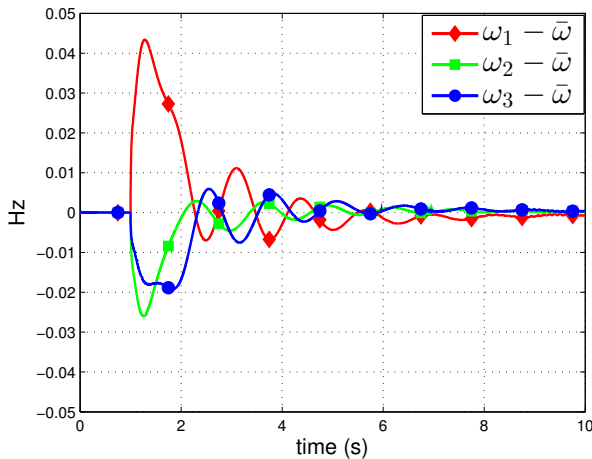


Fig. 12: Frequency deviations with respect to the weighted-average frequency (case P-WAF).

4.3 Overall performance

This section analyses the overall performance of the control strategies regarding:

- rotor-angle stability against large disturbances (transient stability) and
- rotor-angle stability against small disturbances (electromechanical oscillations)

Transient stability is the main application of control strategies P-WAF, Q-WAF and PQ-WAF and it has been analysed in detail in [23, 25]. Nevertheless, results on transient stability are also included in this paper, for reference, to evaluate the overall performance of the control strategies. Transient-stability margins are quantified using the critical clearing time (CCT), which is defined as

the maximum time duration that a fault can stay before clearance without eventually provoking loss of synchronism. An extremely severe fault is selected: a three-phase-to-ground short circuit applied to line 4031-4041a (close to bus 4041) (see Fig. 4), which is cleared by disconnecting the two circuits of the corridor (Fault I, for short). At the initial operating point, each circuit of the corridor carries 644.50 MW.

The impact of communication latency on the performance of the control strategies is also analysed by introducing a delay in the frequency set point calculated by each VSC (τ) when calculating the WAF in (1):

$$\omega^* = \bar{\omega} e^{-\tau s} \quad (6)$$

A second-order Padé's approximation has been used to represent the transfer function of the delay in (6), as proposed in [45]. Realistic values for the delays ($\tau = 50$ ms and $\tau = 100$ ms) were tested [46].

Table 3 shows damping ratios and frequencies of the inter-area modes A and B, and the CCT of Fault I, obtained in the base case and for control strategies P-WAF, Q-WAF and PQ-WAF. In all cases, controller gains are set to $k_{P,i} = k_{Q,i} = 200$ pu and the rest of the parameters as described in the Appendix. The control strategies significantly increase the damping ratios of inter-area modes A and B, in comparison with the base case. The damping ratios deteriorate slightly in the presence of communication latency; however the improvements are still significant. The control strategies increase the CCT of Fault I significantly. Communication latencies do not reduce the CCT in strategy P-WAF. This is consistent with the results presented in [47]: the DC-voltage droop attenuates the effect of communication latency when modulating P injections. However, the impact of communication latency is stronger when modulating Q injections with strategy Q-WAF. Nevertheless, results obtained in the presence of communication latency are better than those obtained in the base case.

Hence, results prove that control strategies P-WAF, Q-WAF and PQ-WAF improve significantly both transient stability and electromechanical-oscillation damping.

Table 3 Comparison. EO: Electromechanical oscillations (small disturbance), TS: Transient stability (large disturbance).

Case	EO		TS Fault I CCT (ms)
	Mode A ζ (%), f (Hz)	Mode B ζ (%), f (Hz)	
Base case	3.23 %, 0.51 Hz	6.10 %, 0.83 Hz	70 ms
P-WAF, $\tau = 0$ ms	19.27 %, 0.62 Hz	17.38 %, 0.89 Hz	270 ms
P-WAF, $\tau = 50$ ms	19.29 %, 0.62 Hz	17.39 %, 0.89 Hz	270 ms
P-WAF, $\tau = 100$ ms	19.30 %, 0.62 Hz	17.39 %, 0.89 Hz	270 ms
Q-WAF, $\tau = 0$ ms	22.24 %, 0.53 Hz	13.18 %, 0.86 Hz	230 ms
Q-WAF, $\tau = 50$ ms	19.37 %, 0.54 Hz	13.06 %, 0.86 Hz	180 ms
Q-WAF, $\tau = 100$ ms	16.09 %, 0.54 Hz	12.73 %, 0.86 Hz	120 ms
PQ-WAF, $\tau = 0$ ms	22.74 %, 0.71 Hz	21.23 %, 0.91 Hz	320 ms
PQ-WAF, $\tau = 50$ ms	19.21 %, 0.70 Hz	21.06 %, 0.91 Hz	300 ms
PQ-WAF, $\tau = 100$ ms	16.75 %, 0.69 Hz	21.06 %, 0.90 Hz	280 ms

5 Conclusions

This paper analysed the impact of transient-stability-tailored supplementary controllers in VSC-MTDC systems on electromechanical-oscillation damping, by means of small-signal stability analysis. In the control strategies analysed, each VSC of the MTDC system compares its own frequency with the weighted-average frequency (WAF) of the VSC stations and it modulates its P injection, Q injection or both simultaneously (P-WAF, Q-WAF and PQ-WAF, respectively).

The conclusions obtained in this paper can be summarised as follows:

- Control strategies P-WAF, Q-WAF and PQ-WAF can be tuned to (a) improve transient stability and to (b) damp inter-area electromechanical oscillations too.

- The control strategies produce good results in the presence of communication delays, under small disturbances and under large disturbances.
- Although bulk power transmission and the recollection of non-dispatchable energy sources are the main purposes of a multi-terminal VSC-HVDC system embedded in a conventional HVAC system, the flexibility of VSC stations makes it possible the contribution of these systems to the overall improvement of the power system stability. This contribution adds a remarkable value to this technology and should be taken into account when carrying out a cost-benefit analysis in future developments.

Appendix A: Data

A.1: Data of the test system

Data of the original CIGRE Nordic32A benchmark test system can be found in [39, 48] and a comprehensive description of the system can be found in [49]. Some modifications were made in the test system used in this paper, in order to stress the system and to reduce the damping ratio of inter-area oscillations. The modifications made are detailed in [19]. Converter and HVDC grid parameters are provided in Table 4.

A.2: Parameters of the control strategies for the case study

- P-WAF: $k_{P,i} = 200$ pu, $\Delta p_{max,i} = 1.0$ pu, $T_{f,i} = 0.1$ s, $T_{W,i} = 10$ s and $\alpha_k = 1/3$. The gains are in nominal p.u. Different values of $k_{P,i}$ are analysed in Section 4.1.
- Q-WAF: $k_{Q,i} = 200$ pu, $\Delta q_{max,i} = 1.0$ pu, $T_{f,i} = 0.1$ s, $T_{W,i} = 10$ s, $V_{TH,i} = 0.75$ pu and $\alpha_k = 1/3$. The gains are in nominal p.u. Different values of $k_{Q,i}$ are analysed in Section 4.1.
- PQ-WAF: The same parameters of strategies P-WAF and Q-WAF are used.

Table 4 Converter & HVDC grid data. Base for pu: VSC's nominal apparent power.

Parameters	
Nominal apparent power	1000 MVA
DC voltage	± 320 kV
AC voltage	300 kV
Configuration	Symmetrical monopole
Active-power limits	± 1000 MW
Reactive-power limits	± 450 MVar
Current limit	1 pu (<i>d</i> -axis priority)
DC-voltage limits	± 10 %
Max. modulation index ($m_i^{max} = \sqrt{\frac{3}{2}} \cdot \frac{V_{dc,B}}{V_{ac,B}}$)	1.31 pu
Current-controller time constant (τ)	5 ms
Connection impedance: $\bar{z}_s = r_s + jx_s$ (reactor + 300/400 kV transformer)	$0.002 + j0.17$ pu
Active-power control	$i_{d,i}^{ref} = p_{s,i}^{ref} / u_{s,i}$
Reactive-power control	$i_{q,i}^{ref} = -q_{s,i}^{ref} / u_{s,i}$
DC-voltage droop parameter ($k_{dc,i}$)	0.1 pu
VSCs' loss parameters (<i>a/b</i>)	$11.033 / 3.464 \times 10^{-3}$ pu
VSCs' loss parameters ($c_{rec} c_{inv}$)	$4.40 / 6.67 \times 10^{-3}$ pu
DC-line series parameters ($R_{dc,ij} / L_{dc,ij}$)	$2.05 \Omega / 140.10$ mH
DC-line shunt capacitance ($C_{cc,ij}$)	1.79 μ F
VSC Eq. capacitance ($C_{VSC,i}$)	193.21 μ F
Total eq. DC-bus capacitance ($C_{dc,i}$)	195.00 μ F

Aknowledgement

This work was supported by the Spanish Government and MCI/AEI/FEDER (EU) under Project Ref. RTI2018-098865-B-C31 and by Madrid Regional Government under PROMINT-CM Project Ref. P2018/EMT-4366.

6 References

- 1 D. Van Hertem and M. Ghandhari, "Multi-terminal VSC HVDC for the European supergrid: Obstacles," *Renewable and Sustainable Energy Reviews*, vol. 14, no. 9, pp. 3156–3163, 2010.
- 2 E. Bompard, G. Fulli, M. Ardelean, and M. Masera, "It's a Bird, It's a Plane, It's a... Supergrid," *IEEE power & energy magazine*, vol. 12, no. 2, pp. 41–50, 2014.
- 3 O. Gomis-Bellmunt, E. Sánchez-Sánchez, J. Arévalo-Soler, and E. Prieto-Araujo, "Principles of Operation of Grids of DC and AC Subgrids Interconnected by Power Converters," *IEEE Transactions on Power Delivery*, vol. 36, no. 2, pp. 1107–1117, 2021.
- 4 G. Buigues, V. Valverde, A. Etxegarai, P. Eguía, and E. Torres, "Present and future multiterminal HVDC systems: current status and forthcoming developments," in *Proc. International Conference on Renewable Energies and Power Quality (ICREPQ)*, Malaga, Spain, 4-6 April, 2017, pp. 83–88.
- 5 A. L. Figueroa Acevedo, A. Jahanbani-Ardakani, H. Nosair, A. Venkatraman, J. D. McCalley, A. Bloom, D. Osborn, J. Caspary, J. Okullo, J. Bakke, and H. Scribner, "Design and valuation of high-capacity HVDC macrogrid transmission for the continental US," *IEEE Transactions on Power Systems*, vol. 36, no. 4, pp. 2750–2760, 2020.
- 6 J. McCalley and Q. Zhang, "Macro Grids in the Mainstream: An International Survey of Plans and Progress," Americans for a Clean Energy Grid (ACEG), Macro Grid Initiative, Tech. Rep., 2020.
- 7 F. del Pizzo, E. M. Carlini, T. Baffa Scirocco, P. Capurso, F. Dicuonzo, C. Armillei, A. Zanghi, and A. Urbanelli, "Towards the Italian electricity grid of the future," in *Proc. CIGRE Session, Paris*, 2022, pp. 1–10.
- 8 Y. Pipelzadeh, B. Chaudhuri, T. C. Green, Y. Wu, H. Pang, and J. Cao, "Modelling and dynamic operation of the Zhoushan DC grid: Worlds first five-terminal VSC-HVDC project," in *Proc. International High Voltage Direct Current 2015 Conference, Seoul, Korea, October 18-22*, 2015, pp. 87–95.
- 9 X. Li, Z. Yuan, J. Fu, Y. Wang, T. Liu, and Z. Zhu, "Nanao multi-terminal VSC-HVDC project for integrating large-scale wind generation," in *Proc. IEEE/PES General Meeting, National Harbor, MD, USA, 27-31 July*, 2014, pp. 1–5.
- 10 G. Bathurst and P. Bordignon, "Delivery of the Nan'ao multi-terminal VSC-HVDC system," in *Proc. 11th IET International Conference on AC and DC Power Transmission (ACDC)*, Birmingham, UK, 10-12 February, 2015, pp. 1–6.
- 11 H. Rao, "Architecture of Nan'ao multi-terminal VSC-HVDC system and its multi-functional control," *CSEE Journal of Power and Energy Systems*, vol. 1, no. 1, pp. 9–18, 2015.
- 12 Z. Zheng, Y. Wang, D. Zhang, R. Song, C. Li, and T. Zhang, "Reliability Evaluation Model of Zhangbei Multi-Terminal HVDC Transmission System," in *Proc. IEEE International Conference on Energy Internet (ICEI)*, Nanjing, China, 27-31 May, 2019, pp. 279–284.
- 13 R. Shah, J. Sánchez, R. Preece, and M. Barnes, "Stability and control of mixed AC-DC systems with VSC-HVDC: a review," *IET Generation Transmission and Distribution*, vol. 12, no. 10, pp. 2207–2219, 2017.
- 14 M. Gu, L. Meegahapola, and K. L. Wong, "Review of Rotor Angle Stability in Hybrid AC/DC Power Systems," in *Proc. IEEE/PES Asia-Pacific Power and Energy Engineering Conference (APPEEC)*, Kota Kinabalu, Malaysia, 7-10 October, 2018, pp. 1–6.
- 15 Y. Pipelzadeh, B. Chaudhuri, and T. C. Green, "Control coordination within a VSC HVDC link for power oscillation damping: A robust decentralized approach using homotopy," *IEEE Transactions on Control Systems Technology*, vol. 21, no. 4, pp. 1270–1279, 2012.
- 16 L. Harnfors, N. Johansson, L. Zhang, and B. Berggren, "Interarea Oscillation Damping Using Active-Power Modulation of Multiterminal HVDC Transmissions," *IEEE Transactions on Power Systems*, vol. 29, no. 5, pp. 2529–2539, 2014.
- 17 R. Preece and J. V. Milanovic, "Tuning of a Damping Controller for Multi-terminal VSC-HVDC Grids Using the Probabilistic Collocation Method," *IEEE Transactions on Power Delivery*, vol. 29, no. 1, pp. 318–326, 2014.
- 18 R. Eriksson, "A New Control Structure for Multi-Terminal dc Grids to Damp Inter-Area Oscillations," *IEEE Transactions on Power Delivery*, vol. 31, no. 3, pp. 990–998, 2016.
- 19 J. Renedo, A. García-Cerrada, L. Rouco, and L. Sigrist, "Coordinated Design of Supplementary Controllers in VSC-HVDC Multi-Terminal Systems to Damp Electromechanical Oscillations," *IEEE Transactions on Power Systems*, vol. 36, no. 1, pp. 712–721, 2021.
- 20 Y. Xing, E. Kamal, B. Marinescu, and F. Xavier, "Advanced control to damp power oscillations with VSC-HVDC links inserted in meshed AC grids," *International Transactions on Electrical Energy Systems*, vol. 31, no. 12, pp. 1–22, 2021.
- 21 R. Eriksson, "Coordinated Control of Multiterminal DC Grid Power Injections for Improved Rotor-Angle Stability Based on Lyapunov Theory," *IEEE Transactions on Power Delivery*, vol. 29, no. 4, pp. 1789–1797, 2014.
- 22 G. Tang, Z. Xu, H. Dong, and Q. Xu, "Sliding Mode Robust Control Based Active-Power Modulation of Multi-Terminal HVDC Transmissions," *IEEE Transactions on Power Systems*, vol. 31, no. 2, pp. 1614–1623, 2016.
- 23 J. Renedo, A. García-Cerrada, and L. Rouco, "Active Power Control Strategies for Transient Stability Enhancement of AC/DC Grids With VSC-HVDC Multi-Terminal Systems," *IEEE Transactions on Power Systems*, vol. 31, no. 6, pp. 4595–4604, 2016.
- 24 H. Latorre, M. Ghandhari, and L. Söder, "Active and reactive power control of a VSC-HVdc," *Electric Power Systems Research*, vol. 78, no. 10, pp. 1756–1763, 2008.
- 25 J. Renedo, A. García-Cerrada, and L. Rouco, "Reactive-Power Coordination in VSC-HVDC Multi-Terminal Systems for Transient Stability Improvement," *IEEE Transactions on Power Systems*, vol. 32, no. 5, pp. 3758–3767, 2017.

- 26 J. C. Gonzalez-Torres, G. Damm, V. Costan, A. Benchaib, and L. Lamnabhi-Lagarigue, "A novel distributed supplementary control of Multi-Terminal VSC-HVDC grids for rotor angle stability enhancement of AC/DC systems," *IEEE Transactions on Power Systems*, vol. 36, no. 1, pp. 623–634, 2021.
- 27 P. Kundur, M. Klein, G. J. Rogers, and M. S. Zywno, "Application of Power System Stabilizers for Enhancement of Overall System Stability," *IEEE Transactions on Power Systems*, vol. 4, no. 2, pp. 614–627, 1989.
- 28 J. Renedo, L. Sigrist, A. García-Cerrada, and L. Rouco, "Modelling of VSC-HVDC multi-terminal systems for small-signal angle stability analysis," in *Proc. 15th IET International Conference on AC and DC Power Transmission*, Coventry, UK, 2019, pp. 1–7.
- 29 S. Cole, J. Beerten, and R. Belmans, "Generalized Dynamic VSC MTDC Model for Power System Stability Studies," *IEEE Transactions on Power Systems*, vol. 25, no. 3, pp. 1655–1662, 2010.
- 30 S. Cole and R. Belmans, "A proposal for standard VSC HVDC dynamic models in power system stability studies," *Electric Power Systems Research*, vol. 81, no. 4, pp. 967–973, 2011.
- 31 J. Beerten, S. Cole, and R. Belmans, "Modeling of Multi-Terminal VSC HVDC Systems With Distributed DC Voltage Control," *IEEE Transactions on Power Systems*, vol. 29, no. 1, pp. 34–42, 2014.
- 32 S. Liu, Z. Xu, W. Hua, G. Tang, and Y. Xue, "Electromechanical Transient Modeling of Modular Multilevel Converter Based Multi-Terminal HVDC Systems," *IEEE Transactions on Power Systems*, vol. 29, no. 1, pp. 72–83, 2014.
- 33 H. Saad, J. Peralta, S. Denetiere, J. Mahseredjian, J. Jatskevich, J. A. Martinez, A. Davoudi, M. Saeedifard, V. Sood, X. Wang, J. Cano, and A. Mehri-Sani, "Dynamic Averaged and Simplified Models for MMC-Based HVDC Transmission Systems," *IEEE Transactions on Power Delivery*, vol. 28, no. 3, pp. 1723–1730, 2013.
- 34 J. Renedo, A. García-Cerrada, L. Rouco, L. Sigrist, I. Egido, and S. Sanz Verdugo, "Development of a PSS/E tool for power-flow calculation and dynamic simulation of VSC-HVDC multi-terminal systems," in *Proc. 13th IET International Conference on AC and DC Power Transmission*, Manchester, UK, 2017, pp. 1–6.
- 35 J. Beerten, S. Cole, and R. Belmans, "Generalized Steady-State VSC MTDC Model for Sequential AC/DC Power Flow Algorithms," *IEEE Transactions on Power Systems*, vol. 27, no. 2, pp. 821–829, 2012.
- 36 F. Milano and A. Ortega, "Frequency divider," *IEEE Transactions on Power Systems*, vol. 32, no. 2, pp. 1493–1501, 2017.
- 37 F. Milano, "Rotor Speed-Free Estimation of the Frequency of the Center of Inertia," *IEEE Transactions on Power Systems*, vol. 33, no. 1, pp. 1153–1155, 2018.
- 38 L. Díez-Maroto, J. Renedo, L. Rouco, and F. Fernández-Bernal, "Lyapunov Stability Based Wide Area Control Systems for Excitation Boosters in Synchronous Generators," *IEEE Transactions on Power Systems*, vol. 34, no. 1, pp. 194–204, 2019.
- 39 M. Stubbe (Convener), "Long Term Dynamics Phase II," Cigré Task Force 38.02.08 - TB 102, Tech. Rep., 1995.
- 40 L. Rouco, "Small Signal Stability Toolbox (SSST): Reference Manual," *Instituto de Investigación Tecnológica (IIT), ETSI ICAI, Universidad Pontificia Comillas, Madrid, Spain*, 2002.
- 41 I. J. Pérez-Arriaga, G. C. Verghese, and F. C. Schweppe, "Selective Modal Analysis With Applications to Electric Power Systems, Part I: Heuristic introduction," *IEEE Transactions on Power Apparatus and Systems*, vol. PAS-101, no. 9, pp. 3117–3125, 1982.
- 42 G. C. Verghese, I. J. Pérez-Arriaga, and F. C. Schweppe, "Selective Modal Analysis With Applications to Electric Power Systems, Part II: The Dynamic Stability Problem," *IEEE Transactions on Power Apparatus and Systems*, vol. PAS-101, no. 9, pp. 3126–3134, 1982.
- 43 F. L. Pagola, I. J. Pérez-Arriaga, and G. C. Verghese, "On Sensitivities, Residues and Participations: Applications to Oscillatory Stability Analysis and Control," *IEEE Transactions on Power Systems*, vol. 4, no. 1, pp. 278–285, 1989.
- 44 M. Klein, G. J. Rogers, and P. Kundur, "A Fundamental Study of Inter-Area Oscillations in Power Systems," *IEEE Transactions on Power Systems*, vol. 6, no. 3, pp. 914–921, 1991.
- 45 Y. Chompoobutrgool and L. Vanfretti, "Analysis of time delay effects for wide-area damping control design using dominant path signals," in *Proc. IEEE/PES General Meeting, National Harbor, MD, USA*, 2014, pp. 1–5.
- 46 F. Zhang, Y. Sun, L. Cheng, X. Li, J. H. Chow, and W. Zhao, "Measurement and Modeling of Delays in Wide-Area Closed-Loop Control Systems," *IEEE Transactions on Power Systems*, vol. 30, no. 1, pp. 2426–2433, 2015.
- 47 J. Renedo, A. García-Cerrada, L. Rouco, and L. Sigrist, "Coordinated Control in VSC-HVDC Multi-Terminal Systems to Improve Transient Stability: The Impact of Communication Latency," *Energies*, vol. 12, pp. 1–32, 2019.
- 48 B. Karlsson, "Comparison of PSSE & PowerFactory," Degree Project, Uppsala Universitet, Uppsala, Sweden, 2013.
- 49 T. Van Cutsem and L. Papangelis, "Description, Modeling and Simulation Results of a Test System for Voltage Stability Analysis," Université de Liège, Belgium, Tech. Rep., 2014.